NTNU

Norwegian University of
Science and Technology

Gearing as a part of an Electric Machine Functionally

Study and optimization of a partitioned stator
switched flux permanent magnet machine

Johan Nicolai Fjellanger

Master of Energy and Environmental Engineering
Submission date: January 2017
Supervisor: Robert Nilssen, IEL
Co-supervisor: Eirik Husum, Rolls-Royce Marine AS in Trondheim

Norwegian University of Science and Technology
Department of Electric Power Engineering

Problem description

Several researchers groups in Europe claim magnetic gearboxes have significant potential as the replacement for mechanical gearboxes in various power conversion systems. One of the developments of magnetic gearing has been to integrate it as a functionally in an electric machine, thus leading to a new class of electric machines – pseudo-direct drives (PDD). It is believed that application of PDD in marine systems, e.g. propulsion units and deck machinery, can be beneficial.

The task is to design such a machine for industrial application, given by Rolls-Royce Marine AS in Trondheim (former SmartMotor AS). Work will include a review of existing magnetic geared machines to choose best topology, and use of FE analysis software for design, evaluation and optimization. The work shall be done in cooperation with engineers at Rolls-Royce Marine AS.

Summary

The idea to couple a gear magnetically has been around for some time, and has gained increased interest in recent years. By manipulating air gap field harmonics, magnetic gearing has been shown to have comparative, or even better performance than its mechanical counterpart, while circumventing typical mechanical disadvantages. Recently, magnetic gearing has been integrated into Permanent Magnet motors to obtain "pseudo" direct-drives that result in efficient high-torque density at low speed electrical machines. This thesis investigates such a promising machine topology, using the Finite Element Analysis tool COMSOL Multiphysics.

The general magnetically geared Partitioned Stator Switched Flux Permanent Magnet machine was found to be able to meet the requested specifications of 200kNm and 4.2MW, with challenges being low power factor and high cogging torque. This machine is a very interesting concept that may be used for low-speed high-torque application when lower power factor can be managed (i.e. power electronics).

Sammendrag

Å koble et gir magnetisk er et gammelt konsept som har fått økt interesse de siste årene. Ved å mainpulere den magnetiske fluxens harmonisitet i luftgapet har det blitt vist at magnetisk giring kan yte tilsvarende eller bedre enn sine mekaniske motstykker, og samtidig unngå typiske mekaniske ulemper. Nylig har konseptet om magnetisk giring blitt integrert i permanentmagnetmotorer, og skapet en «pseudo» direktedrevet maskin. Dette har resultert i mer effektive elektriske maskiner med høyt moment og lav fart. Denne oppgaven undersøker en slik lovende maskintopologi ved bruk av det numeriskt kalkulerende programvareverktøyet COMSOL Multiphysics.
Den generelle oppdelt-stator fluksbyttende permanentmagnetmaskinen har blitt funnet til å være kapabel til å møte målspesifikasjonene på 200kNm og 4.2MW, med utfordringer i høy reaktiv kraftgenerering og momentrippel. Denne type maskin er et lovende og interesant konsept der høy effektivitet behøves ved høy-kraft lav-fart operasjon, og der den reaktive kraftgenereringen kan bli håndtert(f.eks ved bruk av kraftelektronikk.)

Gearing as a part of an Electric Machine Functionally

Johan Nicolai Fjellanger
Department of Electrical Engineering
NTNU - Norwegian University of Science and Technology Trondheim - Norway

***Abstract*—The idea to couple a gear magnetically has been around for some time, and has gained increased interest in recent years. By manipulating air gap field harmonics, magnetic gearing has been shown to have comparative, or even better performance than its mechanical counterpart, while circumventing typical mechanical disadvantages. Recently, magnetic gearing has been integrated into Permanent Magnet motors to obtain "pseudo" direct-drives that result in efficient high-torque density at low speed electrical machines. This thesis investigates such a promising machine topology, using the Finite Element Analysis tool COMSOL Multiphysics.**

The general magnetically geared Partitioned Stator Switched Flux Permanent Magnet machine was found to be able to meet the requested specifications of 200kNm and 4.2MW, with challenges being low power factor and high cogging torque. This machine is a very interesting concept that may be used for low-speed high-torque application when lower power factor can be managed(i.e. power electronics).

***Index Terms*—COMSOL Multiphysics, Permanent Magnet, Partitioned Stator Switched Flux Permanent Magnet, Finite Element Analysis.**

I. Introduction

THE concept of a magnetic gear was conceived more than a century ago, and may be traced back to 1901 when Armstrong designed an electromagnetic spur gear [1]. Traditionally, magnetic gears could not compete with their mechanical counterparts in terms of torque capability [2]. In recent years, publications on magnetic gearing experienced a steep increase around 2008. This may be attributed to cheaper PMs, and that gear topologies are beginning to compete with traditional mechanical gears.

Essentially, a magnetic gear can be designed according to each available topology of its mechanical counterpart. Fig. 1 shows examples of such gears. Magnetic gearing has many advantages such as contact-free, no gear lubrication, high-speed-reduction ratio and high durability. Disadvantages are relatively high cost and potential resource issues when rare earth magnets are used. It becomes increasingly important to consider less or no rare-earth magnet gears and machines.

By the principle of magnetic gearing, many PM machines have been developed with built-in gearing. These machine designs have either incorporated a complete magnetic gear with two arrays of PM, such as the pseudo direct drive [3] and the magnetically geared machine with three air gaps [4]. This thesis will explore such a promising concept presented in [5], the partitioned stator switched flux permanent magnet machine (PS-SFPM). The machine is scaled for industrial application,

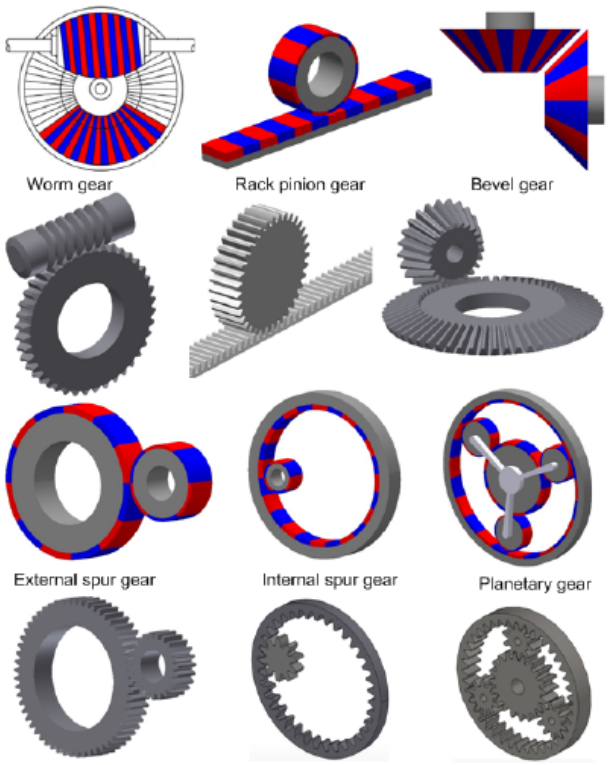

Fig. 1. Corresponding gear topologies between mechanical and magnetic gears.

rated at 1.2m diameter, 200kNm, 200rpm, 4.2MW and 690V 3-phase. This thesis is a building on a specialization project at the Norwegian University of Science and Technology(NTNU) in 2015 by the same author [6].

II. Gearing concepts and magnetic geared machines

A. Traditional gearing

Magnetic gearing is the use of non-fundamental air gap field harmonics to produce constant torque which are a result of modulation of the field due to slotting. To imagine the physics working in such a gear, one can draw many analogies to a mechanical gear. See the external spur gear in Fig. 1. Spinning the larger wheel will make the smaller wheel turn at a faster speed, with a proportional lower torque. Neglecting losses, the power transferred is a one-to-one ratio. The magnetic version functions the same way. Here the cogs are replaced with PMs,

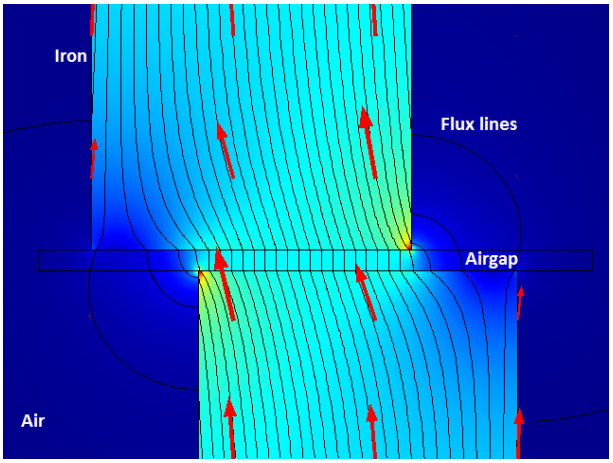

Fig. 2. Magnetic field in two iron cogs. Force is created in the left horizontal direction by the field displacement in the same direction.

transferring power by magnetic coupling, see Fig. 2. As there is no mechanical coupling of torque between bodies, there is no need for lubrication.

One particular advantage of magnetic gearing is its inherent overload protection [7]. When a mechanical gear would be damaged in response to excessive overload, a magnetic gear would harmlessly start slipping, then automatically and safely resume when the fault torque is removed.

In a mechanical gear, power is transferred by physically connecting the cogs of the two wheels together. The coupling is made strong by hard material, such as steel. In a magnetic gear, the magnetic field connects PMs together to transfer power between the moving parts. The coupling is made strong by PMs remanence flux and coercivity.

In traditional gears, coupling elements become very expensive at higher torque for magnetic versus mechanical – steel vs PMs. This is the main reason why magnetic gears struggles to compete with mechanical.

B. Magnetic gearing

A gear transfers power through the coupling elements. In traditional mechanical topologies, this power is unevenly distributed between the coupling elements – cogs or PMs. The coupling elements are never contributing to power transfer at the same time.

However, all the coupling elements may contribute to power transfer in some magnetic gear topologies. This significantly increases achievable torque transmission in a magnetic gear. Such a topology was presented in [9] — Fig. 3. Here the magnetic field acting on the rotating parts is modulated by a set number of iron pieces. This modulation allows either rotor to ”see” a different number of magnetic poles, thus opening the possibility of evenly distributing power transfer across all the coupling pieces – the PMs.

Mechanically this is conceptually similar to epicyclic gearing – the planetary gear in Fig. 4. This study [7] concluded that the magnetic version can be described by the same Willis equations as in the mechanical, wherefore a planetary gear gives

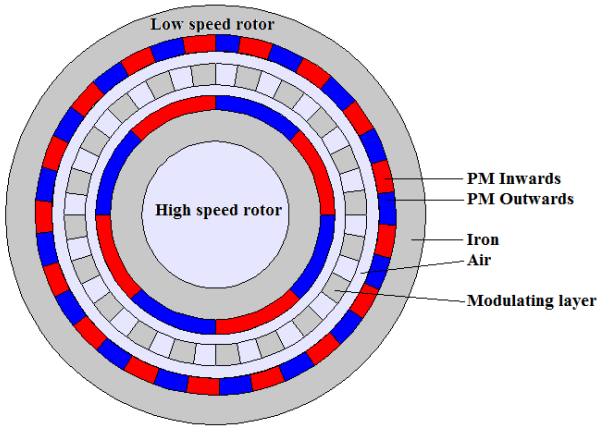

Fig. 3. Magnetic gear with 2 inner PM pole pairs, 16 modulating iron pole pieces and 14 outer PM pole pairs.

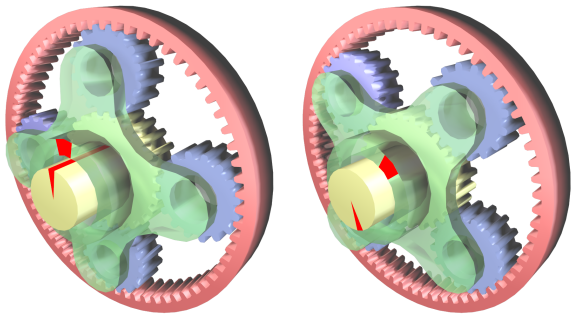

Fig. 4. Planetary gear train consisting of a sun gear (yellow), planet gears (blue) supported by the carrier (green) and a ring gear (pink).

$$N_s\omega_s + N_p\omega_p = (N_s + N_p)\omega_c \tag{1}$$

$$N_r\omega_r + N_p\omega_p = (N_r - N_p)\omega_c \tag{2}$$

Where ω_r, ω_s, ω_p, ω_c is the angular velocity of the ring, sun planetary gear and planetary carrier respectively. N_r, N_s, N_p is the number of the teeth on the ring, sun and planetary gear respectively.

In the magnetic version of the planetary gear train the number of teeth in the ring and sun gear corresponds to pole pairs, and the number of teeth on the carrier corresponds to modulating pole pieces. This is confirmed by combining (1) and (2)

$$P_i\omega_i + P_o\omega_o = (P_i + P_o)\omega_m = N_m\omega_m \tag{3}$$

Where P_i, P_o is the number of pole pairs on the inner and outer rotor, respectively. N_m is the number of modulating pole pieces, and ω_m is the speed of these. For different rotational speeds, maximum transmittable torque occurs when (3) holds. This creates corresponding flux density space harmonics on either side of the two air gaps.

Any combinations of the three parts can rotate to transmit power, but keeping one PM rotor stationary results in the simplest mechanical design, in addition to increasing maximum transmittable torque [9]. Gear ratio then becomes

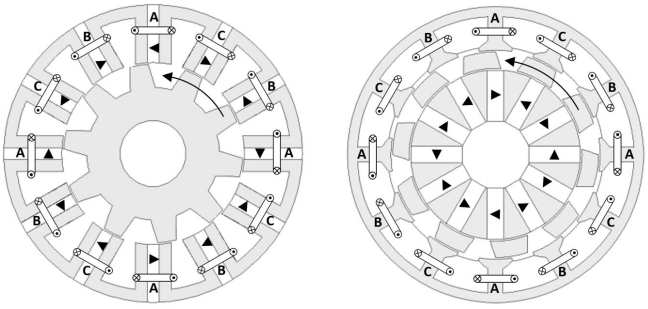

(a) (b)

Fig. 5. 12/10 Slot/Pole. (a) Switched flux machine. (b) Partitioned stator switched flux machine.

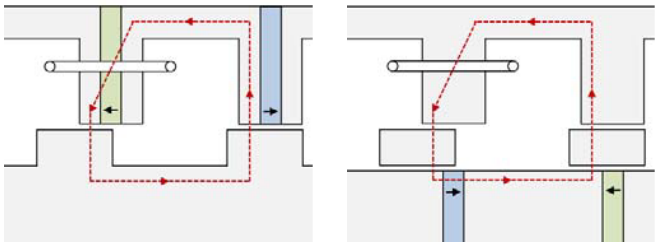

(a) (b)

Fig. 6. (a) Conventional and (b) partitioned stator switched flux machines flux path and PM magnetization direction.

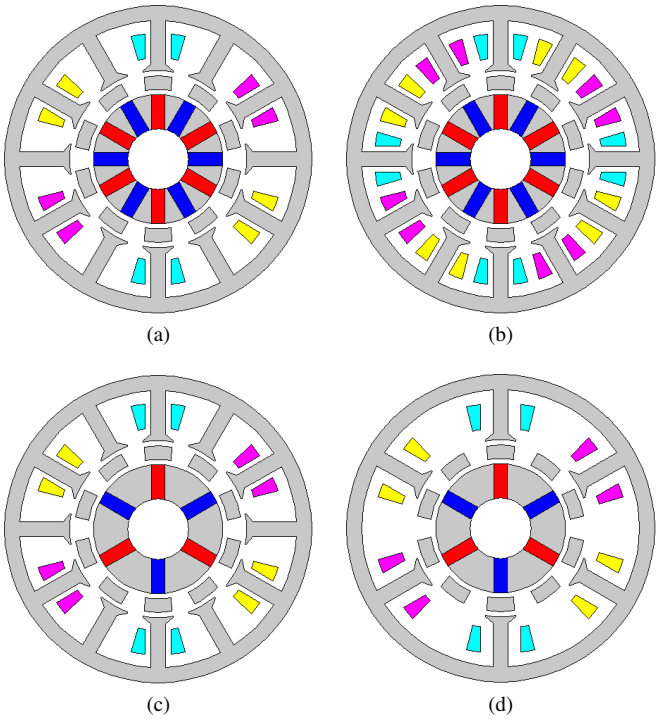

(a) (b) (c) (d)

Fig. 7. Cross section single and double wound 12/10, and E-core and C-core 6/10 slot/pole PS-SFPM. (a) Single wound. (b) Double wound. (c) E-core. (d) C-core.

$$G_r = \frac{N_m}{P_o} \tag{4}$$

C. Integrated magnetic gearing

The magnetic gearing principle can be included in an electric machine either by a two-stage topology, consisting of machine and gear box, or as an integrated functionally in the machine itself. This opens up great possibilities for electrical machines, which typically have poor performance at high-torque low-speed operation — power/weight ratio becomes very low. The rotating PMs in a magnetic gear can be replaced by armature field windings to principally produce the same rotating magnetic field — Fig. 5. We then get a machine that operates on the same principles [12] as a switched flux permanent magnet (SFPM) machine, but with a partitioned stator topology (PS-SFPM) — Fig. 6. Currently, the SFPM machine is extensively researched all over the world [14]. By utilizing a magnetic gearing approach, we may create a highly efficient machine that suppresses its original drawbacks, at the cost of another air gap.

D. Partitioned stator switched flux PM machine

The PS-SFPM machine may be understood from two perspectives: as a magnetically geared machine with inner stationary PMs, rotating modulating poles, and outer stator armature windings. It may also be understood as a switched flux machine with the PMs removed from within the stator teeth, and placed on a secondary stator.

SFPM machines were developed from simple flux-switch alternators [13]. By partitioning the stator, the PS-SFPM machine differs considerably from previous magnetically geared machines since the number of PM poles is equal to the number of stator teeth. This typically results in extremely large cogging torque when PMs are rotating, and would generally be neglected as feasible topology. By having an equal number of modulating poles, stator teeth and interior mounted PM, the flux focusing capability [15] of a SFPM machine is preserved.

The PS-SFPM also benefits from separating PMs and armature windings, allowing increased copper and PM volumes, plus better thermal capabilities as the PMs are removed from the hot copper windings. While maintaining the flux focusing effect, this separation returns the conflict between PM, copper and iron back to the situation in a conventional brushless PM machine, where the air gap diameter determines the ratio of magnetic and electric loading. The main drawback is power factor, due to two air gaps instead of one.

E. Different magnetic geared topologies

Some different PS-SFPM machine topologies are presented in Fig. 7. These machines are a very new concepts, and very little data is available. From the corresponding SFPM machine topologies one can get a general idea of performance, but no more. Uncertainties from partitioning the machine are mainly due to the change of magnetic saturation in the machine, and the added air gap. This thesis will also scale the machine up to $0.6m$ radius, further increasing complexity. As there are most research to be found for the 12/10 PS-SFPM machine, and the

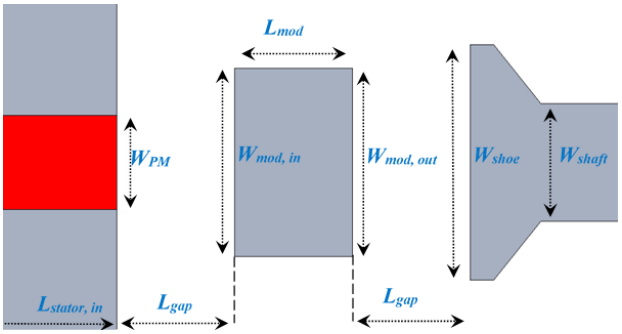

Fig. 8. Important air gap design parameters in the PS-SFPM.

corresponding SFPM machine is well covered in literature, it is chosen for this thesis.

III. Machine Overview

A. Air gap flux density

Accurate prediction of the air gap flux density is important, and can save a lot of computational time. The sub-domain method is often used for this purpose, such as in [17]. However, the gearing effect — interaction between the open-circuit and armature reaction air gap fields — cannot be observed in detail by harmonics analysis via the sub-domain method. Instead a simple magno-motive force(MMF)-permeance model [16] is used in this thesis.

Due to the modulation of the rotor iron pieces to the inner air gap open-circuit PM MMF, complex field harmonics will be produced in the outer air gap. Similarly, field harmonics will be produced in the inner air gap due to the armature reaction MMF. By fourier series expansion of the waveforms in Fig. 9, we can transform these air gap fluxes through the modulating pieces, and express the resulting flux distribution on the opposing side — appendix A. There are both static and rotating field harmonics. This is due to stationary PMs and rotating pole pieces. Further study reveals that some harmonic waves rotate backwards.

From Fig. 5, resulting flux in the outer air gap from the open-circuit PM field is presented in Fig. 10. Notice how the field is transformed from the 6 PM pole pairs to emulating the corresponding 4 pole field of the armature. Similar transformation can be shown for the outer air gap armature reaction flux to the inner air gap flux.

B. Magnetic poles

As previously discussed, the maximum transmittable torque occurs when (3) holds. Similarly, in a magnetic geared machine with P_{pm} PM pole pairs, P_{ph} armature winding pole pairs and N_m, the governing equation is given by

$$P_{ph} + P_{pm} = N_m \tag{5}$$

The magnetic gearing ratio is also expressed similarly to the magnetic gear

$$G = \frac{N_m}{P_{ph}} \tag{6}$$

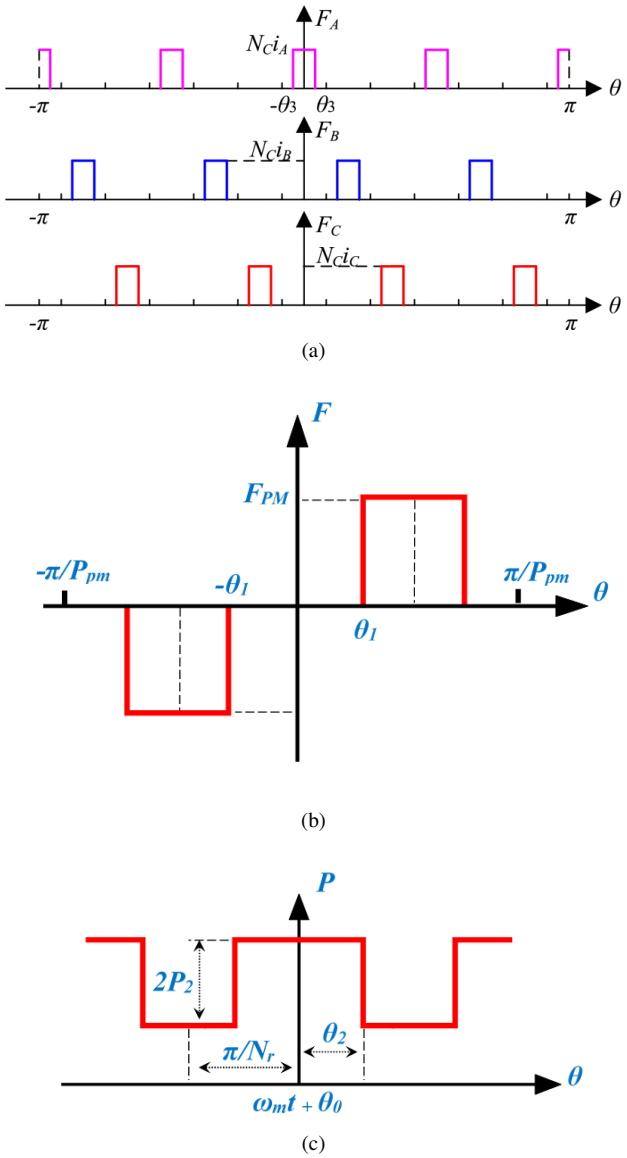

Fig. 9. (a) Outer air gap armature reaction MMF, (b) inner air gap open-circuit MMF, and (c) air gap permeance waveform considering modulating pole pieces.

where G is gear ratio. The gear ratio in this machine is 2.5, same as for the 12/10 slot/pole machine. SmartMotor Trondheim advised to investigate the 24/20 machine for the $0.6m$ radius case, due to concerns regarding magnet topology and structure complexity. In a 12/10 machine with radius $0.6m$ each PM area will be so large that the eddy current losses may be too high. The next level is 36/30 machine, with a complex structure that would be difficult to manufacture.

We have some degrees of freedom to vary N_m by $\pm 1, 2$, creating uneven magnetic balance on the modulating poles. This results in air gap harmonics that may vary back-emf, power factor, torque ripple and maximum torque [16]. However, the effect of $N_m \pm 1, 2, ...$ is far from crippling, and is of great interest, but is out of scope for this thesis. In addition, a machine where (5) holds is expected to be best suited for up-scaling, as magnetic forces on the rotor are the most evenly balanced.

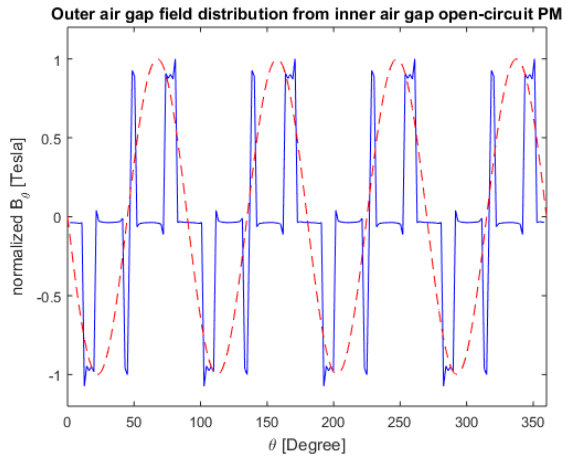

Fig. 10. Open circuit PM field modulated through the pole pieces in Fig. 5. The continuous line is the modulated field waveform in the air gap. The dashed line is its first harmonic. Both waveforms are normalized wrt. themselves.

C. Armature winding

Winding the machine double wound as in Fig. 7b is expected to produce highest average torque [19]. The single wound Fig. 7a produces similar torque at lower coil current densities, but for the same electrical load, as the current density increases, the outer stator teeth becomes more easily saturated. This is because the number of turns per coil is double in the single wound than for the double wound. In terms of efficiency, the double wound is also the better choice, mainly because of the longer end-windings in a single wound machine [18]. It should be mentioned that the E-core in Fig. 7c has lower average torque, and higher cogging, but the best torque per PM volume ratio, likely making it the most cost efficient.

D. Cogging torque

SFPM machines normally exhibits high cogging torque, typically around 10%, so special consideration should be taken for high torque applications [20]. Cogging has shown to be reduced by higher numbers of inner PMs and stator teeth [19], and shaping of the modulation pieces. As will be shown, shaping the rotor pieces — particularly rounding of the inner side corners — reduces cogging greatly, but at the cost of average torque and lower power factor.

E. Power factor

Research on the PS-SFPM is typically interested in torque capabilities, and not much has been done to optimize for the low power factor such machines typically exhibit — around 0.5. Deriving from machines of similar working principle — like the flux-modulated PM synchronous machine in [17] — we can make some assumptions as to what design parameters are important for high power factor. The general situation is that power factor competes with design complexity, mainly in choice of pole numbers and modulation piece shape. In this thesis, the ratios presented in [17] will participate in the design baseline for FEM analysis.

F. Thermal consideration

Thermal considerations in any PM machine is important as to not reach a temperature where the magnets could be demagnetized. Disregarding mechanical, heat appears due to copper losses in the coils, and eddy currents in the PMs and iron. On recommendation by SmartMotor Trondheim, the current density in the coil should be investigated for an upper limit of $J_{max} = 5A/mm^2$.

G. Losses

Disregarding mechanical, losses in an electric machine are divided into copper and core. Approximately, this may be expressed as

$$\begin{cases} W_{loss} = W_{copper} + W_{eddy} + W_{hysteresis} \\ W_{copper} = I^2 R \\ W_{eddy} = K_e f^2 {K_f}^2 {B_m}^2 \\ W_{hysteresis} = K_h f {B_m}^{1.6} \end{cases} \tag{7}$$

where W_{eddy} and $W_{hysteresis}$ are in the Steinmetz equation form, K_h is Steinmetz hysteresis constant, K_e is Steinmetz eddy current constant, B_m is maximum magnetic field strength, and f is frequency of magnetic reversal.

Copper losses becomes a function of coil window area, as the current density and voltage in the coil are to be constant. Larger area increases the losses. This may be counter intuitive, but remember we attempt to maximize magnomotive force at an upper limit of operating temperature. Skin effect is disregarded as each coil wire diameter is sufficiently small (around $6 - 13mm$).

Core losses are caused by eddy currents circulating in resistive materials, and hysteresis losses that occurs when coercive materials are magnetized. Core losses are mainly dependent on the magnetic field strength, and the frequency of which it varies. Copper losses are expected to dominate core losses in the 24/20 machine in this thesis [18]. This is due to the low speed at which this machine will operate.

Calculation of core losses in the iron (iron losses) are not done in this thesis, as Comsol version 5.1 is not modelling this well, and implementing approximate methods such as (7) has low accuracy for anything but the finest meshes. This is mainly because of the utilization of field harmonics in the machine, causing field vectors in each mesh to be nowhere near one-dimensional.

There is a wide variety of alternative calculation methods for hysteresis in FEA available, and the most widely accepted seems to be based on the Jiles-Atherton method [25], taking a very engineering approach to the problem by decomposing magnetization into its reversible and irreversible component. This method is included in the newer Comsol version 5.1a, but not 5.1, which is the tool available for this thesis. However, it is possible to manually implement this in Comsol, but it is very time consuming and requires experience with the materials used in the machine. Accurate iron loss calculations through FEA modelling would be a master thesis in itself, and is therefore only recommended as further work.

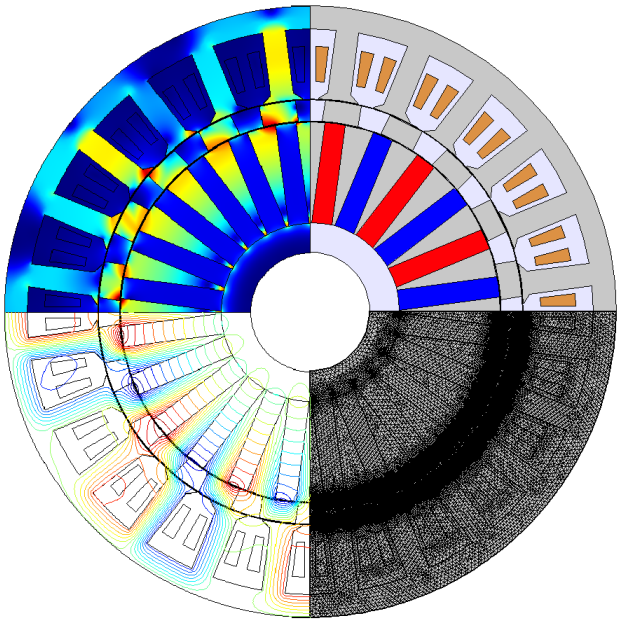

Fig. 11. Comsol PS-SFPM 24/20-machine model visual. Top left: Magnetic flux density. Top right: Geometry. Bottom left: Magnetic flux lines, where red and blue indicate direction. Bottom right: Mesh density overview.

IV. Comsol FEA modeling

COMSOL multiphysics ver. 5.1 was used for FEA analysis in this thesis. Following is a few notes on model set up.

Mode set up was close to an application, meaning all geometric parameters and domains were calculated based on ratios and/or conditionally dependent on one another. For instance, changing machine split ratio would change coil window, which would change the current going through the coil based on maximum current density. This made it possible to preform parametric sweep on every variable.

Model space was two-dimensional, so effects such as coil end has not been accounted for. The "Rotating Machinery, Magnetic" was used for physics node, allowing rotational displacement between mesh domain boundaries. For losses in PMs, they were modelled as single turn coils with zero current in axial direction.

Material parameters for iron domain was lossless soft iron — zero conductivity and nonlinear BH-curve. PMs were modelled as air, with NdFeB-PM remanent flux density $1.2T$ and conductivity $0.667 \cdot 10^6 S/m$.

Torque calculation is built into the Comsol node "Force Calculation", which uses the Maxwell stress tensor along rotor domain boundaries. However, this method proves to be taxing on computational time, and struggles to converge for anything but the finest meshes. Instead, the alternative Arkkios Method [21] was used

$$\begin{cases} T_e = \dfrac{l_a}{\mu_0(r_{\delta,out} - r_{\delta,in})} \displaystyle\int_{r_{\delta,in}}^{r_{\delta,out}} \int_0^{2\pi} rB_r B_\phi dr d\phi \\ rB_r B_\phi dr d\phi = \dfrac{(xB_x + yB_y)(yB_x - xB_y)}{\sqrt{x^2 + y^2}} \end{cases} \tag{8}$$

TABLE I
Machine parameters

Parameter	Unit	Value
Machine diameter	m	1.2
Machine length	m	1
Rotational speed	rpm	200
Rated voltage	V	690
Line frequency	Hz	66.667
Total air gap length	mm	5
Poles		
PM pole pairs	-	12
Stator teeth	-	24
Rotor modulation pieces	-	20
Coils		
Armature phases	-	3
Winding layout	-	Single
Turns per coil	-	28
Coil slot	mm^2	118
Fill factor	-	0.5
Current density	A/mm^2	5
Permanent magnets		
Type	-	NdFeB
Remanent flux density	T	1.2
Conductivity	10^6 S/m	0.667
Length	cm	197.16
Width	cm	45.25
Total magnet area	m^2	0.193

Coils were current controlled with zero d-axis current, and rms current was defined through current density. Coil turns were defined through cross-section of a single wire, and available coil slot area.

Meshing in the machine air gaps were much finer than the rest of the mesh, due to the magnetic field with strong radial component and minuscule variation in tangential component. This change tangential component is paramount for all torque calculations in electric machines.

Solver was a time-dependent study, with a stationary solver to find initial values. The initial value solver was set with lower error tolerance than the time-dependent one. In addition, the Jacobian-matrix produced by Comsol is set to update at every solver iteration, and error estimation was set to exclude algebraic consideration.

V. Optimization of parameters

A. Model geometry

Based on work done for global geometric parameters for high torque in SFPM [22] we can make some well-educated guesses for initial geometric ratios and values, and investigate the applicability of the up-scaled partitioned stator version. Optimization was done with parametric sweep over ratios of logical geometric relationships, presented in II. For instance, stator back iron ratio is expressed with relation to the with of the stator tooth, because of the direct flux path relationship they share. It was found that the machine split ratio — inner

TABLE II
GEOMETRIC RELATIONS

Parameter	Value [cm]	Dependent on	by fraction
Inner stator length	372	Machine radius	0.62
Back-iron length	2.716	PM max width	0.6
PMs			
Max. width	4.525	Pole number	-
Width	4.073	Max width	0.9
Modulating pieces			
Length	4.073	PM width	1
Inner width	7.049	Max. arc span	0.6
Outer width	7.036	Max. arc span	0.54
Corner rounding	Circle radius	Inner width	0.7
Notch depth	0.814	Length	0.2
Stator teeth			
Length	15.512	Remaining length	1
Shaft width	4.525	PM max width	1
Pole shoe width	8.359	Max. arc span	0.6
Shoe-shaft angle	40 [deg]	-	-

stator length to machine length — and modulation piece radial length had the biggest impact on output torque. Appendix B presents some of the data used to arrive at the geometric relations in table II.

It should be noted that the geometry-torque relationship is extremely complex. Each geometric value may or may not influence several machine parameters at once, such as average and cogging torque, power factor, losses, rigidity and thermal limits, to mention a few. Varying one geometric value, while fixing the others is not a good way to numerically determine how to get best performance, but is a good indication of the different geometric relationships in the machine. Examples of this are understanding how much we can reduce back-iron to increase slot area, without affecting overall performance too much, and the effect of shaping the modulating pole pieces and stator teeth. For true optimization, the built-in optimization node in Comsol can be used to check all major machine parameters. The optimization algorithm can be instructed to work on several output variables at once, such as power(torque, losses), performance(power factor, cogging) and cost(PM size). A thorough investigation would require strong computational power, and is therefore only recommended as further work in this thesis.

B. Cogging reduction

The PS-SFPM is a dual air gap machine, trading high torque density for power factor. The air gap should be made as small as possible, but is limited by high cogging torque. We can suppress this by changing machine geometry, such as shaping the rotor pieces, and adding a shoe to the stator teeth to more evenly distribute flux. Based on work on SFPM in [24] and [23] this thesis concludes with the rotor piece and pole shoe shape presented in Fig. 12. In this thesis, several other rotor piece shapes have been investigated, such as different notching schemes, chamfering(cutting) and/or filleting(rounding) of edges, in addition to giving the inner stator — the PMs — a

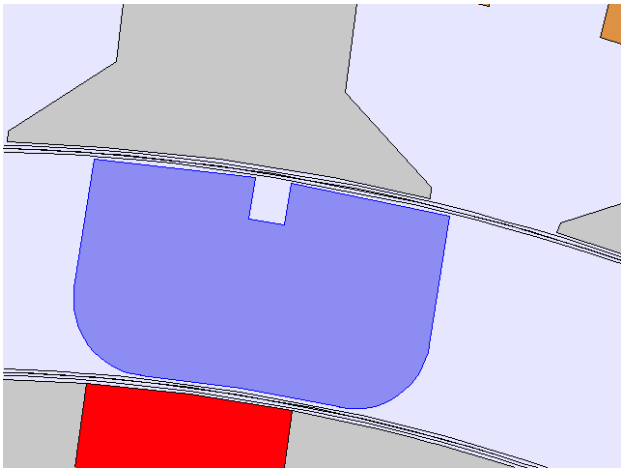

Fig. 12. Shaping of air gap geometry to reduce cogging.

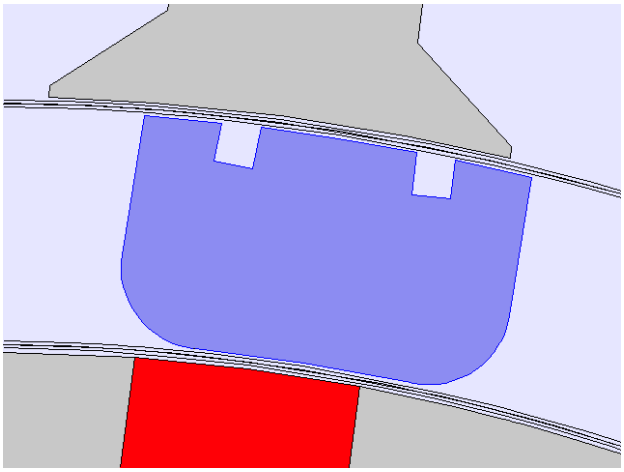

Fig. 13. One of the alternative notching schemes investigated.

shoe structure, similar to the outer stator teeth. All of these schemes reduced cogging, but were very taxing on average torque. In terms of ripple as a percentage of average torque, the shapes in Fig. 12 seems to be the better option.

VI. SIMULATED PERFORMANCE

Machine key performance values are presented in table III, and data graphics in Fig. (14) and (15). Table III contains both the improved and unimproved geometry for ripple performance. The ripple becomes smaller, but at the cost of average torque, and an even lower power factor. In both cases, the specifications given in the introduction of 200kNm and 4.2MW can be met by increasing the length of the machine from $1m$ to approximately $1.8m$, as both torque and power theoretically are linearly dependent on machine length. SmartMotor Trondheim provided an upper limit of $2.4m$ machine length, so this is well within reason, apart from slightly higher power rating.

Machine losses appears accurate, as the difference between mechanical and electric power is not far from the combined coil and PM losses.

TABLE III
MACHINE PERFORMANCE
BASE CASE, AND IMPROVED RIPPLE GEOMETRY

Parameter	Unit	Unimproved	Improved
Average torque	kNm	122.15	108.79
Torque ripple	kNm	8.24	5.98
(Peak-to-peak)	%	6.8	5.5
Electric power	MW	2.682	2.410
Mechanical power	MW	2.556	2.278
Coil losses	kW	67.743	67.743
PM losses	kW	55.142	63.155
Efficiency	%	95.30	94.50
Power factor	-	0.518	0.463

From Fig. 15 we see there are some numerical instability. This is most likely caused by the looser constraints on error estimation set in the solver. These constraints are necessary for Comsol to model PMs as a single-turn coil. By comparing different solver settings — with and without single-turn modelled PMs — this effect was found to be very small.

VII. CONCLUSION

This thesis investigated a new magnetically geared machine topology, scaled up for marine industrial use. The general PS-SFPM machine was found to be able to meet the specifications of 200kNm and 4.2MW, with challenges lying in the low power factor and cogging torque. The PS-SFPM is a very interesting concept that may be used for low-speed high-torque application when lower power factor can be managed(i.e. power electronics).

The load-torque curve in Fig. 14 shows a curve that is only beginning to flatten out. As the coil current density upper limit is set to a very safe value ($5A/mm^2$), there is still potential for higher torque. Further work should include a thermal study to determine what loads the machine — especially the PMs — can handle.

Further work should also include numerical investigation of iron losses, and/or building a prototype for testing losses experimentally. As the rotor is made of nothing but steel, several rotors could theoretically be easily made for the same prototype, investigating different shapes and pole numbers.

If a powerful computer can be made available, a thorough optimization algorithm should be run for the machine geometric parameters, as discussed in section V-A.

VIII. ACKNOWLEDGMENT

The author would like to thank supervisors Prof. Robert Nilsen and Eirik Mathias Husum, and research assistant Hallvar Haugdal for their guidance through this work.

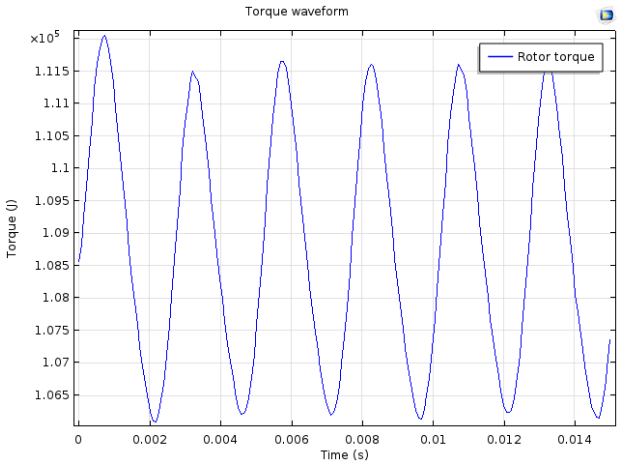

(a)

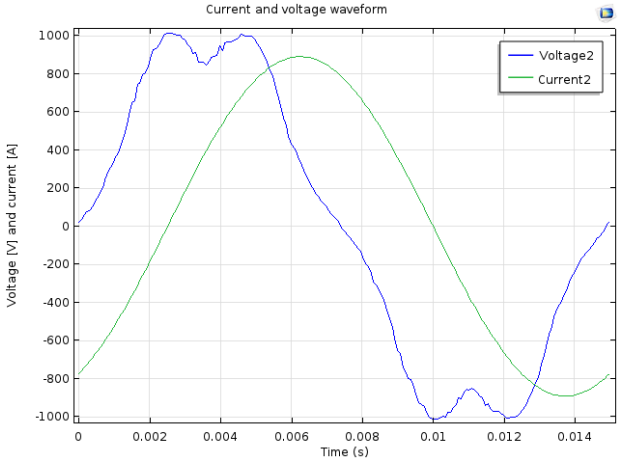

(b)

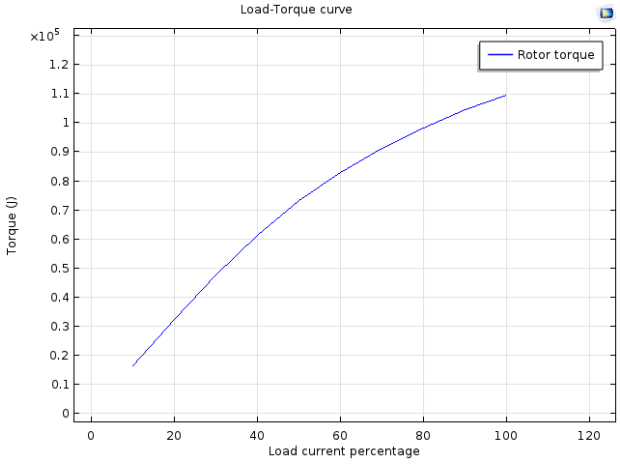

(c)

Fig. 14. (a) Torque waveform. (b) Voltage and current waveforms of one phase. (c) Load-Torque curve.

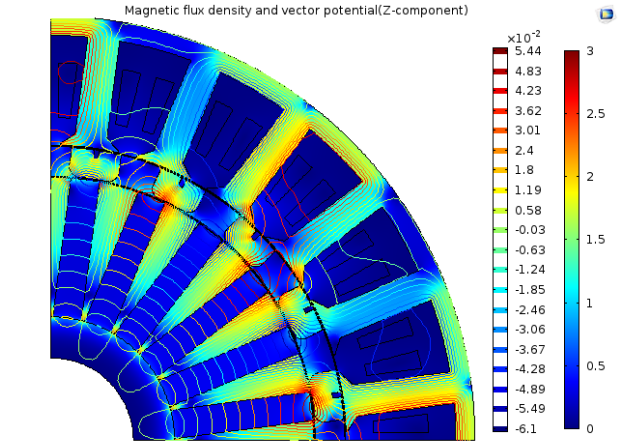

(a)

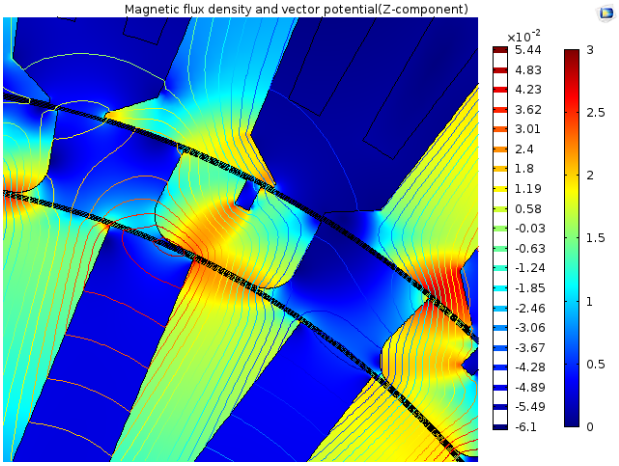

(b)

Fig. 15. Flux density graphics. (a) Quarter of the machine. (b) Air gap zoom. Colours of flux density have units [T], and flux vector potential [Wb/m].

REFERENCES

[1] C. G. Armstrong, "Power transmitting device," US Pat. 687 292, 1901.

[2] S. Kikuchi and K. Tsurumoto, "Design and characteristics of a new magnetic worm gear using permanent magnet," Magnetics, IEEE Transactions on, vol. 29, no. 6, pp. 29232925, 1993.

[3] K. Atallah, J. Rens, S. Mezani, and D. Howe, "A novel pseudo direct drive brushless permanent magnet machine," IEEE Trans. Magn., vol. 44, no. 12, pp. 4605-4617, Dec. 2008.

[4] K. T. Chau, Z. Dong, J. Z. Jiang, L. Chunhua, and Z. Yuejin, "Design of a magnetic-geared outer-rotor permanent-magnet brushless motor for electric vehicles," IEEE Trans. Magn., vol. 43, no. 6, pp. 2504-2506, Jun. 2007.

[5] Z.Q. Zhu and D. Evans, "Overview of Recent Advances in Innovative Electrical Machines", Department of Electronic and Electrical Engineering, University of Sheffield, UK, Oct. 2014.

[6] J. Fjellanger, "Gearing as a part of an Electric Machine Functionally," Specialization project, NTNU, Dec. 2015.

[7] E. Gouda, S. Mezani, L. Baghli, and A. Rezzoug, "Comparative study between mechanical and magnetic planetary gears," IEEE Trans. Magn., vol. 47, no. 2, pp. 439-450, Feb. 2011.

[8] P.M. Tlali, R-J. Wang, S. Gerber, "Magnetic gear technologies: a review, Stellenbosch, Western Cape, South Africa, December 2015.

[9] K. Atallah, S. D. Calverley, and D. Howe, "Design, analysis and realization of a high-performance magnetic gear," IEE Proc. EPA, vol. 151, no. 2, 2004, pp. 135-143.

[10] J. Pyrhonen, T. Jokinen, and V. Hrabovcova "Design of Rotating Electrical Machines, John Wiley and Sons Ltd, 2008, pp 34.

[11] D. Li, R. Qu, J. Li, W. Xu, and L. Wu, "Synthesis of flux switching permanent magnet machines," IEEE Trans. Energy Convers., vol. 31, no. 1, pp. 106117, Mar. 2016.

[12] D. J. Evans and Z. Q. Zhu, "Novel partitioned stator switched flux permanent magnet machines," IEEE Trans. Magn., vol. 51, no. 1, Jan. 2015, Art. no. 8100114.

[13] S. E. Rauch and L. J. Johnson, "Design principles of flux-switch alternators" Trans. Amer. Inst. Elect. Eng. Power Appl. Syst., vol. 74,

[14] Z. Q. Zhu, "Switched flux permanent magnet machines - innovation continues" Int. Conf. Elect. Mach. and Syst. (ICEMS), Keynote Speech paper, Aug. 20-23. 2011, pp. 1-10. no. 3, pp. 12611268, Jan. 1955.

[15] J. T. Shi, Z. Q. Zhu, D. Wu, and X. Liu , "Influence of flux focusing on electromagnetic torque of novel biased flux PM machines," ICEM, Nov. 2015.

[16] Z. Z. Wu, Z. Q. Zhu, "Analysis of Magnetic Gearing Effect in Partitioned Stator Switched Flux PM Machines," IEEE Trans. on En. Conv., vol. 31, no. 4, December 2016.

[17] X. Zhang, X. Liu, J. Liu, and Z. Chen, "Analytical investigation on the power factor of a flux-modulated permanent-magnet synchronous machine," IEEE Trans. Magn., vol. 51, no. 11, Nov. 2015.

[18] D. Evans, Z. Zhu, Z. Wu, H, Zhan, X. Ge, "Comparative analysis of parasitic losses in partitioned stator switched flux PM machines with double- and single-layer windings," IEMCD, May 2015.

[19] C. Awah, Z. Zhu, Z. Wu, H. L. Zhan, J. T. Shi, D. Wu, X. Ge, "Comparison of Partitioned Stator Switched Flux Permanent Magnet Machines Having Single- and Double-layer", IEEE Trans. Magn., vol. 51, no. 1, Jan. 2016.

[20] D. Wang , X. Wang , and S. Jung, "Reduction on Cogging Torque in Flux-Switching Permanent Magnet Machine by Teeth Notching Schemes," IEEE Trans. Magn., vol. 48, no. 11, Nov 2012.

[21] J. Pyrhonen, T. Jokinen, and V. Hrabovcova "Design of Rotating Electrical Machines", John Wiley and Sons Ltd, 2008, pp 34.

[22] Z. Zhu, Y. Pang, J. Chen, Z. Xia, D. Howe, "Influence of Design Parameters on Output Torque of Flux-Switching Permanent Magnet Machines," IEEE VPPC, Sept. 2008.

[23] C. Sikder, I. Hsain, W. Ouyang, "Cogging torque reduction in Flux-Switching Permanent-Magnet machines by Rotor Pole Shaping," IEEE Trans. on ind. app., vol. 51 no. 5, Sept. 2015.

[24] J. Hu, L. Wang, J. Zou, B. Zhao, "Cogging Torque Reduction of Hybrid Excitation Flux Switching Motor," Fifth international conference on instrumentation and measurement, comp., comm, and ctrl, 2015.

[25] N. Sadowski, N. Batistela, J. Bastos, M. Lajoie-Mazenc,"An Inverse Jiles-Atherton Model to Take Into Account Hysteresis in Time-Stepping Finite-Element Calculations", IEEE Trans. on Magn. vol. 38, no. 2, march 2002.

APPENDIX A
AIR GAP FLUX DENSITY EQUATIONS

[16] Fourier series of outer air gap MMF based on 3-phase coil current exitation, Fig. 9a

$$\begin{cases} F_{ABC}(\theta,t) = \dfrac{3\sqrt{2}N_c I_{rms}}{\pi}\displaystyle\sum_{i=1}^{\infty}\frac{\sin(4i\theta_1)}{i}\sin(\xi_i) \\ \xi_i = \begin{cases} -4qi\theta + N_m\omega_m t, & i \in [1,4,7,...] \\ 4qi\theta + N_m\omega_m t, & i \in [2,5,8,...] \\ 0, & i \in [3,6,9,...] \end{cases} \end{cases} \tag{9}$$

where F_{ABC} is the 3-phase armature reaction MMF. N_c is the number of coil turns. θ_1 is half of tooth shoe arc. ω_m is the rotor mechanical angular speed. q is a constant equal to 1 and 2 in a 12/10-pole and 24/20-pole PS-SFPM machine respectively.

Fourier series of inner air gap MMF, Fig. 9b

$$\begin{cases} F_{pm}(\theta) = \dfrac{4}{\pi}\hat{F}_{pm}\displaystyle\sum_{j=1}^{\infty}\frac{\cos(a_j P_{pm}\theta_2)}{a_j}\sin(a_j P_{pm}\theta) \\ a_j = 2j-1 \end{cases} \tag{10}$$

where F_{pm} is the PM MMF. $\hat{F}_{pm}$ is the constant PM MMF value. P_{pm} is the PM pole pair number. θ_2 is half of the PM arc θ_{pm}.

Fourier series of Air gap permanence waveform, Fig. 9c

$$\begin{cases} P(\theta,t) = P_0 + \dfrac{4P_2}{\pi}\displaystyle\sum_{k=1}^{\infty}\frac{sin(kN_m\theta_3)}{k}\cos(\phi) \\ \phi = kN_m(\theta - \omega_m t - \theta_0) \end{cases} \tag{11}$$

where P_0 is the DC component of air gap permeance. P_2 is the peak-to-peak component of air gap permeance. θ_3 is half of the modulating pole piece arc θ_m.

Multiplying (10) and (11) gives the outer air gap open-circuit PM flux density distribution

$$\begin{cases} B_{PMout}(\theta,t) = P_0\dfrac{4}{\pi}F_{pm}\displaystyle\sum_{j=1}^{\infty}\frac{\cos(a_j P_{pm}\theta_2)}{a_j}\sin(a_j P_{pm}\theta) \\ +\dfrac{8F_{pm}P_2}{\pi^2}\displaystyle\sum_{j=1}^{\infty}\sum_{k=1}^{\infty}M_{j,k}(\cos\alpha_1 + \cos\alpha_2) \\ M_{j,k} = \dfrac{\cos(a_j P_{pm}\theta_1)\sin(kN_m\theta_3)}{a_j k} \\ \alpha_1,\alpha_2 = [kN_m \pm a_j P_{pm}]\left[\theta - \dfrac{kN_m(\omega_m t + \theta_0) \pm \frac{\pi}{2}}{kN_m \pm a_j P_{pm}}\right] \\ a_j = 2j-1 \end{cases} \tag{12}$$

Multiplying (9) and (11) gives the inner air-gap armature reaction flux density distribution

$$\begin{cases} B_{ABCin}(\theta,t) = P_0\dfrac{3\sqrt{2}N_c I_{rms}}{\pi}\displaystyle\sum_{i=1}^{\infty}\frac{\sin(4c_i\theta_1)}{c_i}\cos(b_i) \\ +P_2\dfrac{6\sqrt{2}N_c I_{rms}}{\pi^2}\displaystyle\sum_{i=1}^{\infty}\sum_{k=1}^{\infty}O_{i,k}(\cos\beta_1 + \cos\beta_2) \\ O_{i,k} = \dfrac{\sin(4c_i\theta_1)\sin(kN_m\theta_1)}{c_i k} \\ \beta_1,\beta_2 = \\ [kN_m \mp 4qc_i]\left[\theta - \dfrac{(k-1)N_m\omega_m t + kN_m\theta_0 \pm \frac{\pi}{2}}{kN_m - 4qc_i}\right] \\ b_i = 4qc_i\theta - N_m\omega t + \dfrac{\pi}{2} \\ c_i = 3i-2 \end{cases} \tag{13}$$

APPENDIX B
MODEL GEOMETRY INFLUENCE ON OUTPUT TORQUE

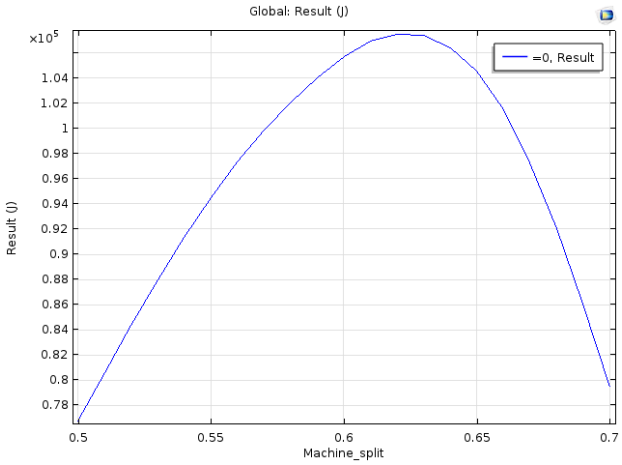

(a)

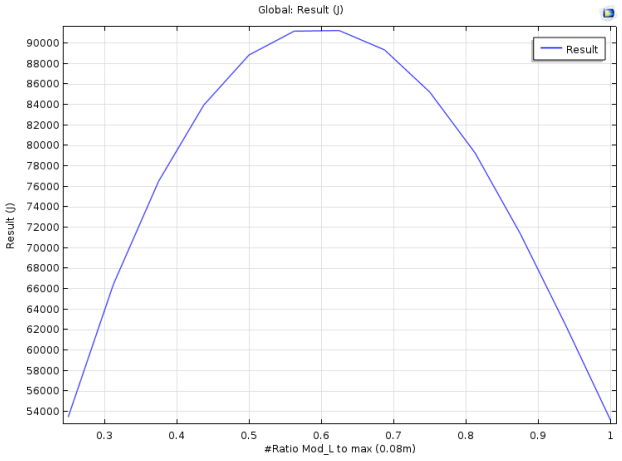

(b)

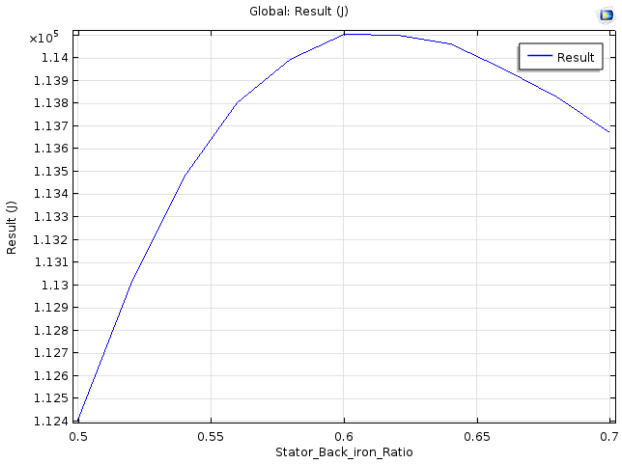

(c)

Fig. 16. Output torque optimization data. (a) Machine split, inner stator to machine length ratio. (b) Length of modulation piece. (c) Stator back iron to tooth width ratio.

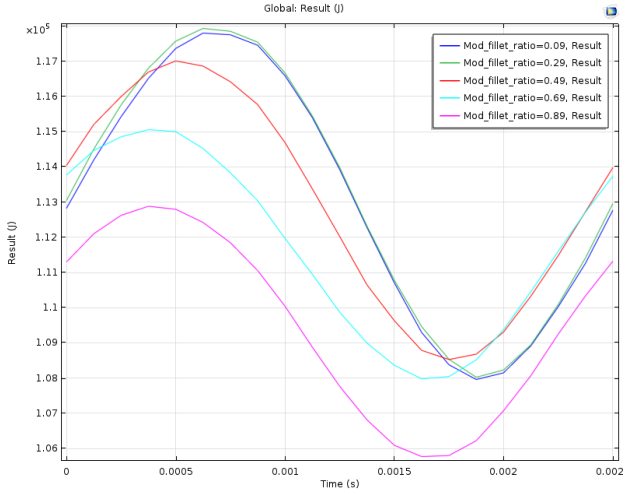

(a)

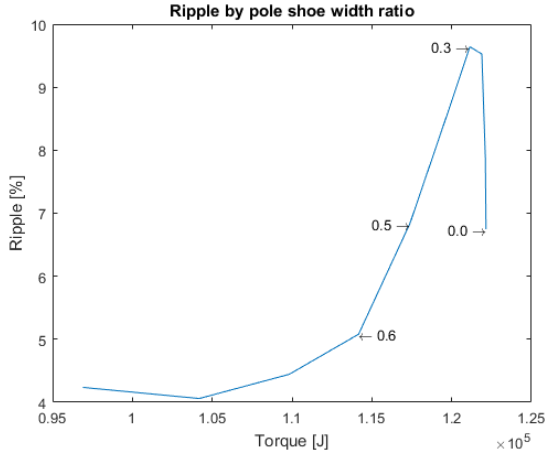

(b)

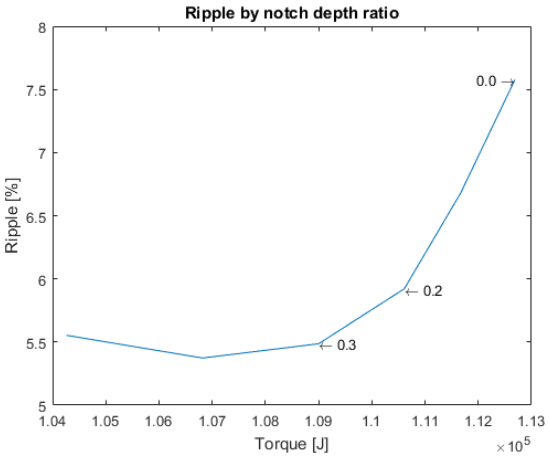

(c)

Fig. 17. Cogging torque optimization data. (a) Rounding of modulating piece. Ratio depicts the rounding circle radius to half of the modulating piece width. (b) Pole shoe width resulting torque and ripple. Ratio depicts pole shoe width to max. pole shoe width. (c) Notching of the modulating piece. Ratio depicts depth of notch to modulating piece length.